Bone 129 (2019) 115056

Contents lists available at ScienceDirect

Bone

journal homepage: www.elsevier.com/locate/bone

Full Length Article

IDH2 deficiency increases bone mass with reduced osteoclastogenesis by limiting RANKL expression in osteoblasts

Suk Hee Lee[a,b], Seung-Hoon Lee[a,b], Jin Hyup Lee[c], Jeen-Woo Park[d], Jung-Eun Kim[a,b,*]

[a] Department of Molecular Medicine, Cell and Matrix Research Institute, School of Medicine, Kyungpook National University, Daegu 41944, Republic of Korea
[b] BK21 Plus KNU Biomedical Convergence Program, Department of Biomedical Science, Kyungpook National University, Daegu 41944, Republic of Korea
[c] Department of Food and Biotechnology, Korea University, Sejong 30019, Republic of Korea
[d] School of Life Sciences and Biotechnology, College of Natural Sciences, Kyungpook National University, Daegu 41566, Republic of Korea

ARTICLE INFO

Keywords:
IDH2
High bone mass
RANKL
Osteoblast-to-osteoclast crosstalk

ABSTRACT

Mitochondria are not only responsible for cellular energy production but are also involved in signaling, cellular differentiation, cell death, and aging. Mitochondrial $NADP^+$-dependent isocitrate dehydrogenase (IDH2) catalyzes the decarboxylation of isocitrate to α-ketoglutarate, accompanied by NADPH production. IDH2 plays a central role in mitochondrial function in multiple cell types and various organs, including the heart, kidneys, and brain. However, the function of IDH2 in bone tissue is yet to be elucidated. Here, we report that disruption of IDH2 in mice results in high bone mass due to decreased osteoclast number and resorption activity. Although IDH2 played no cell-intrinsic role in osteoclasts, IDH2-deficient animals showed decreased serum markers of osteoclast activity and bone resorption. Bone marrow stromal cells/osteoblasts from *Idh2* knockout mice were defective in promoting osteoclastogenesis due to a reduced expression of a key osteoclastogenic factor, receptor activator of nuclear factor-κB ligand (RANKL), in osteoblasts in vivo and in vitro through the attenuation of ATF4-NFATc1 signaling. Our findings suggest that IDH2 is a novel regulator of osteoblast-to-osteoclast communication and bone metabolism, acting via the ATF4-NFATc1-RANKL signaling axis in osteoblasts, and they provide a rationale for further study of IDH2 as a potential therapeutic target for the prevention of bone loss.

1. Introduction

Bone is a highly dynamic tissue that is continuously remodeled to attain and maintain optimal bone integrity, mass, and strength [1–3]. Bone remodeling is tightly regulated by an equilibrium between osteoclast-mediated bone resorption and osteoblast-mediated bone formation [4–6]. An osteopetrotic phenotype develops from a dysregulation of osteoclast differentiation or function and is characterized by a markedly high bone mass [7–9]. In contrast, osteoporotic diseases are associated with an increase in osteoclast-mediated bone resorption and are characterized by marked bone loss [10,11].

Osteoclast differentiation and bone resorption occur via molecular intercellular communication between osteoblasts and osteoclasts that regulates the commitment, proliferation, and differentiation of bone cell precursors [12,13]. Although the mechanisms controlling osteoblast-to-osteoclast crosstalk are not completely elucidated, cytokines secreted by osteoblasts and neighboring stromal cells play a dominant role in osteoclast differentiation, including macrophage colony-stimulating factor (M-CSF), receptor activator for NF-κB ligand (RANKL), and its soluble decoy receptor osteoprotegerin (OPG) [14,15].

Mitochondria are the powerhouses of the cell that provide energy (ATP) for cell function. A significant amount of ATP is consumed during bone remodeling, and its generation is regulated by cell type and is temporally specific [16]. Previous studies have elucidated that mitochondria also play a critical role in the differentiation of multiple cell types [17,18]. In both osteoclasts and osteoblasts, robust mitochondrial biogenesis and supercomplex formation are observed during differentiation, accompanied by increased ATP production [19–22]. Consistent with these findings, mitochondrial dysfunction, characterized by a loss of ATP production efficiency, is closely related to alterations in bone formation [23–25].

Mitochondrial $NADP^+$-dependent isocitrate dehydrogenase (IDH2) is an evolutionarily conserved protein that catalyzes the oxidative decarboxylation of isocitrate, which is involved in ATP production, through the production of α-ketoglutarate (α-KG) in the tricarboxylic

* Corresponding author at: Department of Molecular Medicine, Cell and Matrix Research Institute, School of Medicine, Kyungpook National University, 680 Gukchaebosang-ro, Jung-gu, Daegu 41944, Republic of Korea.
E-mail address: kjeun@knu.ac.kr (J.-E. Kim).

https://doi.org/10.1016/j.bone.2019.115056
Received 13 June 2019; Received in revised form 30 August 2019; Accepted 30 August 2019
Available online 31 August 2019

acid (TCA) cycle [26–28]. Moreover, IDH2 participates in regulating mitochondrial oxidative stress by catalyzing the production of NADPH [29]. Hence, IDH2 is a pivotal factor in mitochondrial function as one of the metabolic enzymes for ATP generation and as a donor of NADPH for redox balance in multiple cell types and various organs, including the heart, kidneys, and brain [30–32]. It is well known that ATP is a signaling molecule that regulates several cellular activities that control gene expression in bone cells [33–35]. ROS are reported to act as intracellular signaling mediators for osteoclast differentiation [36,37] and are involved in osteogenic gene expression in osteoblasts [38–40]. Therefore, a normal mitochondrial function that maintains the proper levels of ATP and ROS is critical for balanced bone metabolism. Although there is mounting evidence that the disruption of IDH2 causes abnormal levels of ATP and ROS and contributes to overall mitochondrial dysfunction, an understanding of the physiological associations between IDH2 and bone metabolism and the underlying mechanisms is lacking.

In the present study, we investigated the role of IDH2 in bone formation and remodeling using mice harboring a targeted disruption of IDH2. These mice undergo normal skeletal development but exhibit high bone mass in vertebrae and long bones due to a significant reduction in both osteoclast number and activity. IDH2 deficiency significantly decreased RANKL expression in the early stage of osteoblast differentiation of primary bone marrow stromal cells. Consistent with these findings, co-culture with osteoblasts derived from IDH2-deficient mice lowered the differentiation capacity of bone marrow-derived osteoclast progenitors. Inactivation of IDH2 was linked to reduced RANKL expression through the activating transcription factor 4-nuclear factor of activated T-cells c1 (ATF4-NFATc1) signaling pathway, acting partly via mitochondrial ATP generation. Our findings provide the first evidence of physiological control of bone metabolism by IDH2 via osteoblast-osteoclast communication that is in turn modulated, at least in part, by RANKL expression in osteoblasts. Moreover, IDH2-deficient mice were protected from ovariectomy-induced bone resorption by the decrease in osteoclastic bone catabolism and the downregulation of RANKL expression. These results suggest that IDH2 is a potential therapeutic target in the treatment of bone loss diseases, such as osteoporosis.

2. Materials and methods

2.1. Animals

All animal procedures were reviewed and approved by the Ethics Committee of Kyungpook National University Institutional Animal Care (Approval No. KNU-2016-0093; Daegu, Korea). The mice used in this study were Idh2 germline knockouts (*Idh2*$^{-/-}$) and their littermates wild-type (WT, *Idh2*$^{+/+}$) mice with a complete C57BL/6 background. The mice were bred and maintained in climate-controlled, specific pathogen-free conditions with a 12 h light/dark cycle and were allowed free access to water and standard mouse chow. The mice were genotyped using PCR, as previously described [41]. The final age of all mice used for analysis was 16 weeks.

2.2. Microcomputed tomography (μCT)-based analysis of bone structure

The structure of long bones was evaluated using μCT with the SkyScan 1272 scanner (Bruker, Kontich, Belgium) at School of Dentistry, Kyungpook National University (Daegu, Korea). Briefly, femurs were collected from female mice at 16 weeks of age, cleaned to remove any soft tissues, fixed in 4% paraformaldehyde (PFA), and rinsed with phosphate-buffered saline (PBS). The fixed femurs were scanned using a high-resolution μCT. The X-ray tube voltage was 60 kV with a current of 166 μA and a 0.25-mm thick Al filter. The exposure time was 424 ms, and the image pixel size was 10 μm. The acquired μCT images were analyzed using the Comprehensive TeX Archive Network (CTAN) topographic reconstruction software (Bruker) to evaluate bone parameters. For bone analysis, a region of 0.7–2.3 mm was selected as the region of interest (ROI) in each image, and image information was obtained based on computed automatic domain values. Trabecular bone mineral density (BMD), bone volume per tissue volume (BV/TV), trabecular bone thickness (Tb.Th), trabecular number (Tb.N), and trabecular separation (Tb.Sp) were measured and calculated.

2.3. Bone histomorphometry analysis

For bone histological analysis, mice were first intraperitoneally injected with calcein green (30 mg/kg; Sigma, St. Louis, MO), then with alizarin red S (60 mg/kg; Sigma) 6 days later. The mice were sacrificed 2 days after the alizarin red S injection. Undecalcified lumbar vertebrae were embedded in destabilized methyl-methacrylate after dehydration by an ethanol series and were cut into 5-μm sections. Fluorochrome images, double-labeled by calcein and alizarin red S, were visualized using a fluorescence microscope at a magnification of 20×. Sections were stained with von Kossa/van Gieson staining to assess mineralized bone, or with toluidine blue to analyze the number of osteoblasts on the bone surface. Tartrate-resistant acid phosphatase (TRAP) staining in osteoclasts was conducted using a Leukocyte TRAP Kit (Sigma), according to the manufacturer's instructions. Finally, static and dynamic bone histomorphometry analyses were performed using BioQuant image analysis software (Bio-Quant, Inc., San Diego, CA).

2.4. Serum analysis

Serum samples were collected from *Idh2*$^{-/-}$ and *Idh2*$^{+/+}$ mice at 16 weeks of age and assayed for bone degradation markers, e.g., CTX-1, using commercially available enzyme-linked immunosorbent assay (ELISA) kits (RatLaps™ EIA, Tyne & Wear, UK), according to the manufacturer's instructions. The levels of OPG and RANKL in mouse serum and osteoblast culture supernatants were measured using Quantikine ELISA kits (R&D Systems, Minneapolis, MN), according to the manufacturer's instructions.

2.5. Cell culture and in vitro differentiation

Bone marrow was harvested from the femur and tibia of 16-week-old mice by centrifugation (10 s at 8000 ×*g*). Whole marrow cells were cultured in cell culture plates in Minimum Essential Medium Alpha Modifications (α-MEM) for 20 h. For the primary osteoclasts, non-adherent cells were collected by density gradient centrifugation using Histopaque-1077 (Sigma) and were seeded in 96-well plates at a density of 2×10^4 cells/well. Differentiation was induced by the addition of M-CSF (20 ng/ml; PeproTech, Rocky Hill, NJ) and RANKL (20 ng/ml; R&D Systems) to the culture medium. The medium was refreshed every other day. For the primary osteoblasts, cells attached to the bottom of the plate were cultured for 5 more days before being seeded in 24-well plates at a concentration of 8×10^4 cells/well. Osteoblastic differentiation was induced in medium supplemented with 10 mM β-glycerophosphate and 100 μg/ml L-ascorbic acid (Sigma). Both osteoclasts (days 0 and 5 with differentiation media) and osteoblasts (days 0, 7, and 14 with differentiation media) were harvested in TRIzol for RNA isolation and in radioimmunoprecipitation assay (RIPA) buffer (Sigma) for protein extraction. TRAP staining was conducted for the visualization of differentiated osteoclasts, and TRAP-positive multinucleated cells (MNCs) were counted using i-Solution image analysis software (IMT i-solution, Daejeon, Korea). For actin ring staining, osteoclasts were fixed in 4% PFA, permeabilized in 0.1% Triton X-100, rinsed in PBS, and immunostained with TRIC-conjugated phalloidin (Invitrogen, Carlsbad, CA). To analyze osteoclast resorption activity, 2×10^4 cells of bone marrow macrophages were cultured on bone slices with differentiation medium. Resorption pits were visualized by staining with Mayer's hematoxylin solution (Sigma) after cells were eliminated, and

the resorption area was measured using the threshold method in ImageJ software (NIH, Bethesda, MD, USA). For the mineralization assay, osteoblast cells cultured for 7 or 14 days were fixed with 4% PFA and then stained with alizarin red S for 10 min at room temperature. Cultures were then washed three times with distilled water before capturing images. The alizarin red stain was dissolved with 10% cetylpyridinium chloride (Sigma) for 15 min at room temperature, and the optical density of the solution at 562 nm was measured using a spectrophotometer. For osteoblast-mediated osteoclast generation, bone marrow cells were cultured in an equal mixture of growth medium and osteoblast-conditioned medium (CM) or co-cultured with osteoblasts plated on 0.4-μm Transwell tissue culture inserts. The cells were then fixed with 4% PFA and stained with TRAP before counting TRAP-positive MNCs.

2.6. RNA isolation, RT-PCR, and quantitative PCR (qPCR)

Total RNA was extracted from cells using TRIzol (Invitrogen). To isolate total RNA from bone homogenates, the femurs and tibias from *Idh2*$^{-/-}$ and *Idh2*$^{+/+}$ mice were harvested. The bone marrow was flushed with PBS and pulverized in TRIzol using a TissueLyser (Qiagen, Valencia, CA). RNA was purified using the RNeasy Micro Kit with DNase I (Qiagen), according to the manufacturer's instructions, and cDNA was generated with 1 μg of total RNA and a reverse transcription premix (Elpis Biotech, Daejeon, Korea). PCR reactions were performed to assay for the presence of *Idh2* and qPCRs were run in triplicate on a 7900HT sequence detector (Applied Biosystems, Foster City, CA) using SYBR Green (Life Technologies, Carlsbad, CA, USA). The mRNA expression of each gene of interest was normalized to that of *Gapdh*. The primer sequences used in this study are listed in Table S1.

2.7. Protein extraction and immunoblotting

Long bone tissue samples were snap-frozen in liquid nitrogen and disrupted in a TissueLyser (Qiagen) with RIPA buffer. For whole-cell lysates, cells were lysed in RIPA buffer. The samples were incubated on a rotator at 4 °C for 30 min and then centrifuged at 12,000 rpm for 10 min at 4 °C. The resulting supernatants were collected. The protein concentrations of the supernatants were measured using a bicinchoninic acid assay (BCA) assay (Pierce, Rockford, IL). Proteins (30 μg/lane) were separated by SDS-PAGE and then transferred to a polyvinylidene difluoride membrane (Immunobilon-P; Millipore, Milford, MA) using a Bio-Rad wet transfer system. The membranes were then blocked with 5% skim milk for 1 h at room temperature before incubating overnight with antibodies against IDH2 (Abcam, Cambridge, MA); p-ATF4 and ATF4 (Thermo Scientific, Waltham, MA); and NFATc1, RANKL, or β-actin (Santa Cruz Biotechnology, Dallas, TX). Signals were detected using a horseradish peroxidase-conjugated secondary antibody and an enhanced chemiluminescence detection kit (ECL; GE Healthcare Life Science, UK).

2.8. Evaluation of mitochondrial damage

The mitochondrial membrane potential was visualized by using rhodamine-123 (Invitrogen) according to the manufacturer's instructions. Briefly, after 3 days of differentiation, the cells were treated with 5 μM rhodamine-123 for 20 min at 37 °C. The fluorescence intensity was measured and analyzed. The mitochondrial ROS level was measured using the MitoSOX Red fluorescent dye (Invitrogen). Cells were differentiated for 3 days, washed with PBS, and incubated with 10 μM MitoSOX Red for 20 min at 37 °C. Fluorescence was evaluated using a Zeiss Axiovert 200 inverted microscope (Oberkochen, Germany).

2.9. ATP and cyclic AMP (cAMP) measurement

The ATP and cAMP levels in cultured osteoblasts were measured using an ATP colorimetric/fluorometric assay kit and a cAMP direct immunoassay kit (Abcam), respectively, according to the manufacturer's instructions. Briefly, 1×10^6 cells were harvested, lysed in 200 μl of ATP assay buffer, and centrifuged at 12,000 rpm for 5 min at 4 °C. The supernatant was deproteinized using ice-cold 4 M perchloric acid and 2 M KOH. For the cAMP assay, cultured osteoblasts were scraped and dissociated completely, and centrifuged for at 12,000 rpm for 10 min. Collected supernatants were then processed directly for cAMP concentration. Values were normalized to the protein concentrations obtained using Bradford assays and expressed as pmol/μg protein.

2.10. Ovariectomy (OVX)

Bilateral OVX and sham operations were performed on female mice at 8 weeks of age. Briefly, OVX was performed under general anesthesia by making a single 0.5-cm long midline dorsal skin incision. Using artery forceps, the ovarian fat pad was gently parted, and the ovaries were exposed. After removing both ovaries, the fat pad was repositioned into the abdomen. The wound was closed by suturing the muscle layer with a single stitch and the skin layer with sterile stainless-steel wound clips. The sham control mice underwent the same procedure, except for ovary removal. The surgically removed ovaries were examined histologically to verify successful OVX. At the age of 16 weeks, mice were sacrificed by cardiac puncture. The success of OVX was also confirmed based on the absence of ovaries and uterine atrophy at sacrifice.

2.11. Immunohistochemistry for RANKL detection

Paraffin sections of femur (5-μm thick) were prepared for RANKL immunolabeling. Briefly, following deparaffination and rehydration with xylene and serial dilutions of ethanol, respectively, the sections were treated with preboiled citrate buffer (pH 6.0) for antigen retrieval for 30 min. Next, incubation with 0.3% hydrogen peroxide was performed for 30 min to inactivate endogenous peroxidase, and then the sections were incubated in blocking solution (10% normal goat serum in PBS) for 1 h to reduce non-specific staining. The sections were then incubated overnight at 4 °C with mouse anti-RANKL antibody (Santa Cruz Biotechnology) at a dilution of 1:100 in PBS containing 1% bovine serum albumin (BSA). After washing with PBS, the sections were incubated with horseradish peroxidase-conjugated rabbit anti-mouse IgG (Thermo Scientific) for 1 h at room temperature. The sections were then rinsed with PBS three times and treated with diaminobenzidine (DAB) (Dako, Glostrup, Denmark) to visualize the immunoreaction. All sections were counterstained with hematoxylin and observed under a light microscope (Leica, Wetzlar, Germany).

2.12. Statistical analysis

All data are expressed as mean ± SD. Means were compared using Student's *t*-test. The significance level was set at $P < 0.05$.

3. Results

3.1. Idh2$^{-/-}$ mice exhibit increased bone mass

To determine the role of IDH2 in bone metabolism, *Idh2* mRNA and protein expression were examined in *Idh2*$^{+/+}$ osteoblasts and osteoclasts derived from bone marrow stromal cells and macrophages, respectively. Both cell types expressed *Idh2*, and the expression level in osteoblasts was significantly higher than that in osteoclasts (Supplementary Fig. S1A, B). As differentiation progressed, *Idh2* mRNA expression decreased in osteoblasts and increased in osteoclasts (data not shown). However, in *Idh2*$^{-/-}$ mice, bone development was not altered by the lack of IDH2, as indicated by the normal longitudinal

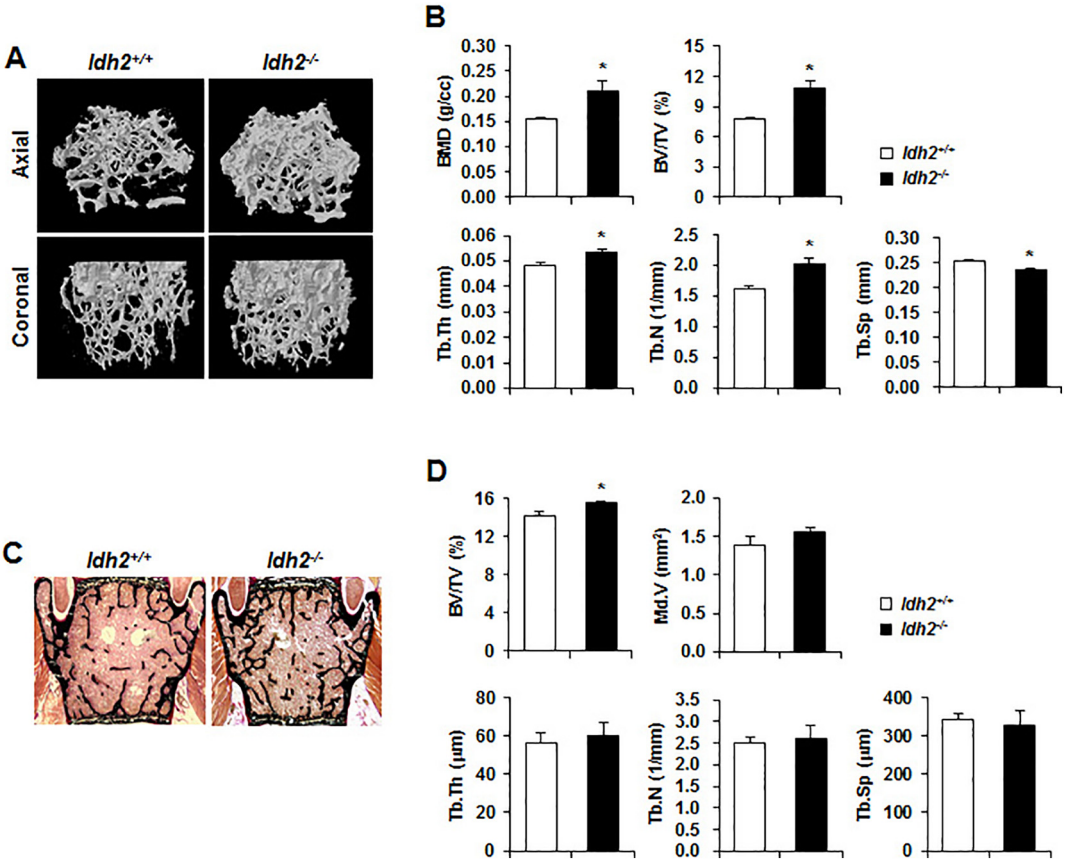

Fig. 1. Bone mass is increased in *Idh2*$^{-/-}$ mice. (A) μCT analysis based on 3D reconstructed images of axial and coronal sections of the distal femur in WT (*Idh2*$^{+/+}$) or *Idh2*-knockout (*Idh2*$^{-/-}$) mice. (B) Trabecular BV and architecture were assessed by μCT. BMD, bone mineral density; BV/TV, bone volume per tissue volume; Tb.Th, trabecular bone thickness; Tb.N, trabecular number; and Tb.Sp, trabecular separation. (C) Lumbar vertebrae sections were stained with von Kossa/van Gieson staining and (D) the following parameters were measured: BV/TV; Md·V, mineralized volume; Tb.Th; Tb.N; and Tb.Sp. Data are represented as the mean ± standard deviation (SD); $n = 6$ per group. *$P < 0.05$ versus control.

bone growth seen in 12-week-old mice (Supplementary Fig. S1C). Next, we analyzed bone mass in 16-week-old mice by μCT of the femur (Fig. 1A, B). Trabecular BMD was significantly increased in *Idh2*$^{-/-}$ mice compared to WT (*Idh2*$^{+/+}$) littermate controls. The μCT analysis also showed an increase in BV/TV due to a significant increase in Tb.Th and Tb.N, and a decrease in Tb.Sp in *Idh2*$^{-/-}$ mice. Histological analysis of lumbar vertebrae sections with von Kossa/van Gieson staining and quantification using BioQuant software confirmed these findings, showing that BV/TV was increased in *Idh2*$^{-/-}$ mice relative to *Idh2*$^{+/+}$ mice (Fig. 1C, D). Moreover, cortical bone thickness was increased in *Idh2*$^{-/-}$ mice compared to *Idh2*$^{+/+}$ mice (Supplementary Fig. S1D). Taken together, these results indicate that IDH2 deficiency results in high bone mass in both the femur and the spine. This increase in bone mass was detected in *Idh2*$^{-/-}$ mice after 16 weeks, and no significant difference was evident when the bone mass was compared in younger mice (data not shown). These results indicate that the higher bone mass in adult *Idh2*$^{-/-}$ mice is likely to result from alterations in bone remodeling, which reflects the balance between bone formation and resorption.

3.2. Bone resorption is reduced in *Idh2*$^{-/-}$ mice

To determine whether the balance between bone formation and resorption is altered, and to identify the underlying cellular mechanism leading to the increased bone mass in adult *Idh2*$^{-/-}$ mice, bone histomorphometry was performed. We first examined the bone formation parameters in the L3 and L4 lumbar vertebrae. Osteoblast number (Fig. 2A upper panel and 2B left graph), mineral apposition rate, and bone formation rate (Fig. 2C) were not altered in *Idh2*$^{-/-}$ mice compared to those in *Idh2*$^{+/+}$ mice, indicating that the osteoblast characteristics are not substantially changed as a result of IDH2 deficiency. In addition, in vitro differentiation of isolated bone marrow stromal cells into osteoblasts showed no difference between the two genotypes, as evidenced by qPCR, which shows comparable mRNA expression levels of the osteoblast markers *Runx2*, *Alp*, *Col1*, and *osteocalcin* (Supplementary Fig. S2A), and comparable alkaline phosphatase staining (Supplementary Fig. S2B). Finally, in vitro mineralization detected by alizarin red S staining on days 7 and 14 of osteoblast differentiation does not differ considerably between the two genotypes (Supplementary Fig. S2C). IDH2 is present in osteoblast lineage cells (Supplementary Fig. S1), but it is not critical for the differentiation or mineralization of osteoblasts (Supplementary Fig. S2). Therefore, the increased bone mass in the adult *Idh2*$^{-/-}$ mice could not be caused by alterations in bone formation, suggesting that bone resorption may be affected. Indeed, fewer osteoclasts were detected in tartrate-resistant acid phosphatase (TRAP)-stained lumbar vertebrae from adult *Idh2*$^{-/-}$ mice than in vertebrae from *Idh2*$^{+/+}$ mice (Fig. 2A lower panel). The quantification of TRAP-positive osteoclasts on the bone surface revealed a 40% decrease in the number of osteoclasts in *Idh2*$^{-/-}$ mice (Fig. 2B right graph). Serum levels of C-terminal telopeptides of type 1 collagen (CTX-1), a marker of osteoclast activity and bone resorption, were also reduced in *Idh2*$^{-/-}$ mice (Fig. 2D). These data indicate that bone resorption activity is decreased, with a reduced number of osteoclasts in *Idh2*$^{-/-}$ mice, which also explains the increased bone mass observed. However, in vitro osteoclast differentiation of bone marrow macrophages of *Idh2*$^{-/-}$ mice was not significantly altered

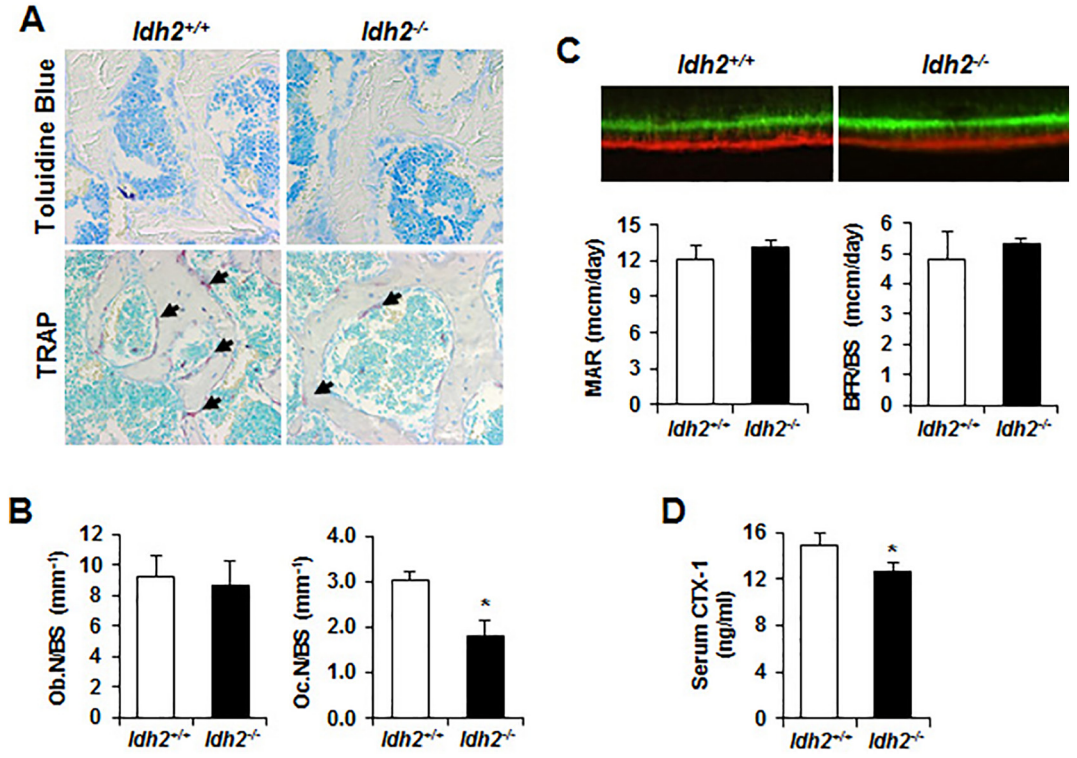

Fig. 2. Bone resorption is decreased in *Idh2*$^{-/-}$ mice. Bone histomorphometry analysis of lumbar vertebrae from *Idh2*$^{+/+}$ and *Idh2*$^{-/-}$ mice (n = 4 per group). (A) Tissue sections were stained with toluidine blue for osteoblasts (upper) or with TRAP for osteoclasts (lower, arrow), and (B) osteoblast number (Ob.N) and osteoclast number (Oc.N) per bone surface were calculated. (C) Representative images of calcein-alizarin red labeling on the unstained tissue section, and the measurements of mineral apposition rate (MAR) and bone formation rate (BFR) based on the images. (D) Serum concentrations of CTX-1 in *Idh2*$^{+/+}$ and *Idh2*$^{-/-}$ mice (n = 6). Data are represented as the mean ± SD. *P < 0.05 versus control. (For interpretation of the references to colour in this figure legend, the reader is referred to the web version of this article.)

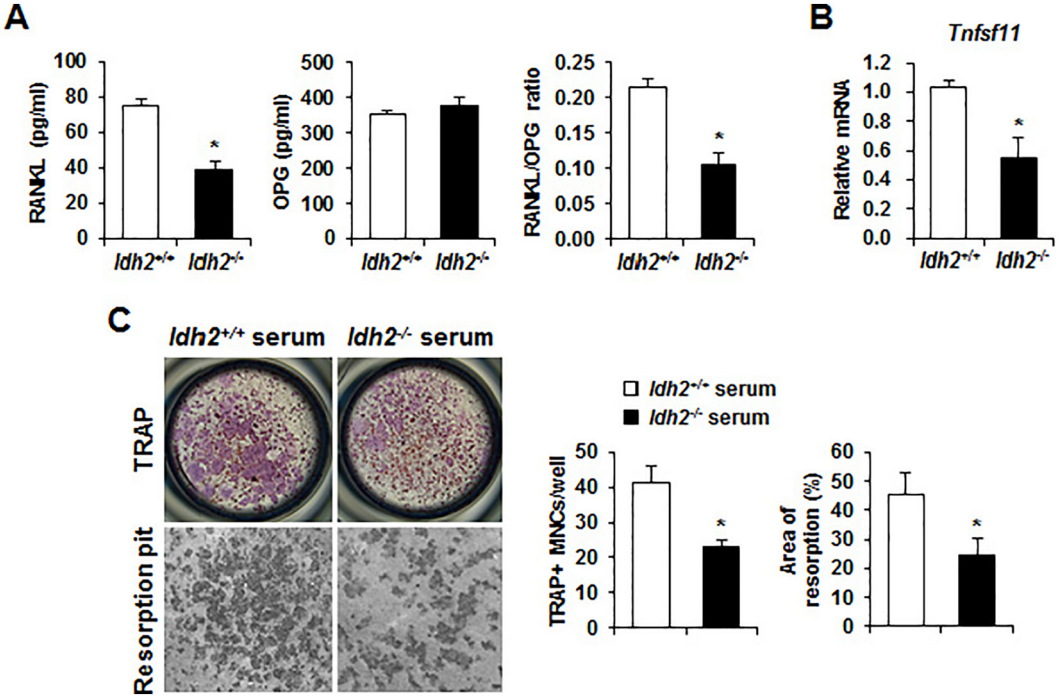

Fig. 3. IDH2 deficiency diminishes RANKL expression in vivo, and osteoclast differentiation and resorption activity are reduced in co-culture with *Idh2*$^{-/-}$ mouse serum. (A) Serum RANKL and OPG levels, and the RANKL/OPG ratio (n = 6 per group). (B) In vivo bone marrow expression of *Tnfsf11* (encoding RANKL) quantified by qPCR. (C) TRAP staining of WT bone marrow macrophages cultured in osteoclast differentiation medium with serum from *Idh2*$^{+/+}$ or *Idh2*$^{-/-}$ mice. TRAP^{+} MNCs containing more than three nuclei were counted. Osteoclast resorption activity was assessed by culturing osteoclasts on bone slices and measuring the resorption area using ImageJ software. Data are represented as the mean ± SD. *P < 0.05 versus control.

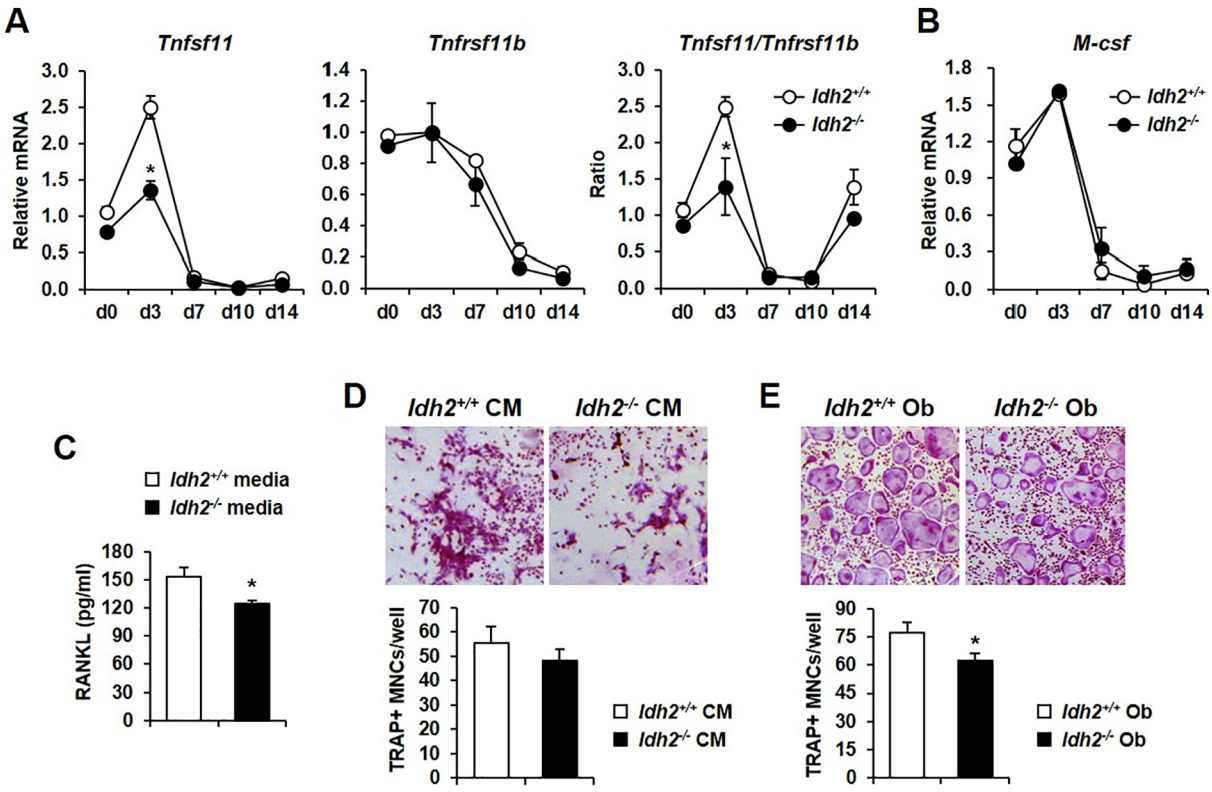

Fig. 4. Multinucleated osteoclast formation is repressed when bone marrow macrophages are cultured with conditioned medium from *Idh2*$^{-/-}$ osteoblasts or co-cultured with *Idh2*$^{-/-}$ osteoblasts. (A) *Tnfsf11* and *Tnfrsf11b* (encoding OPG) expression in primary osteoblasts from bone marrow on days 0, 3, 7, 10, and 14 of differentiation and the calculated ratio. (B) *M-csf* expression in primary osteoblasts on days 0, 3, 7, 10, and 14 of differentiation. (C) RANKL secreted on day 3 from *Idh2*$^{+/+}$ or *Idh2*$^{-/-}$ osteoblasts cultured in differentiation medium as measured by ELISA. (D) TRAP staining of WT bone marrow macrophages cultured with either *Idh2*$^{+/+}$ or *Idh2*$^{-/-}$ osteoblast-conditioned medium (CM) collected on day 3 of differentiation and the number of TRAP^{+} MNCs containing more than three nuclei. (E) TRAP staining of WT bone marrow macrophages co-cultured with either *Idh2*$^{+/+}$ or *Idh2*$^{-/-}$ primary osteoblasts (Ob) and the number of TRAP^{+} MNCs containing more than three nuclei. Data are represented as the mean ± SD of three independent experiments conducted in triplicate. *$P < 0.05$ versus control.

(Supplementary Fig. S3A, B); the functional activity of these osteoclasts was also comparable to that of their WT cells (Supplementary Fig. S3C, D).

3.3. RANKL/OPG serum levels are reduced in Idh2$^{-/-}$ mice

Because bone marrow macrophages from *Idh2*-deficient mice displayed normal osteoclast differentiation and resorptive function in vitro, we next aimed to elucidate the mechanisms by which IDH2 expression in osteoblasts/stromal cells may control osteoclast differentiation. Since RANKL and its decoy receptor, OPG, modulate osteoclastogenesis, and both proteins are produced by osteoblasts/stromal cells, we measured the serum and bone marrow levels of RANKL and OPG. In *Idh2*$^{-/-}$ mice, the RANKL/OPG ratio in serum was half that measured in the serum of WT mice due to a low RANKL concentration (Fig. 3A). The expression of the RANKL-encoding gene, *Tnfsf11*, was also decreased in the bone marrow of *Idh2*$^{-/-}$ mice relative to that seen in WT mice (Fig. 3B). Treatment with serum from *Idh2*$^{-/-}$ mice decreased the differentiation and resorption activities of bone marrow macrophages cultured in osteoclast differentiation medium (i.e., in the presence of RANKL and M-CSF) compared to treatment with serum from WT mice (Fig. 3C).

3.4. IDH2 disruption suppresses RANKL expression in the early stages of osteoblast differentiation and inhibits osteoclastogenesis

Primary bone marrow-derived osteoblasts lacking IDH2 showed significantly reduced *RANKL* mRNA expression in the early stages of differentiation on day 0 and 3 in vitro, while mRNA levels of the anti-osteoclastogenic factor *OPG* were similar between cells isolated from *Idh2*$^{-/-}$ and WT mice (Fig. 4A). The mRNA expression level of *M-CSF,* another critical cytokine for osteoclast differentiation and produced by osteoblasts, showed no significant difference between *Idh2*$^{-/-}$ and *Idh2*$^{+/+}$ mice (Fig. 4B). Consistent with this finding, RANKL protein expression was decreased in the culture medium of *Idh2*$^{-/-}$ osteoblasts on day 3 of differentiation compared to that seen in the culture medium of WT osteoblasts (Fig. 4C). To determine the ability of *Idh2*-deficient osteoblasts/stromal cells to support osteoclastogenesis, we performed co-culture experiments. Since the lack of IDH2 in osteoblasts resulted in decreased RANKL expression, we hypothesized that co-culturing with primary osteoblasts isolated from *Idh2*$^{-/-}$ mice would suppress osteoclastogenesis in WT osteoclast precursors (bone marrow macrophages in primary culture). WT osteoclast precursors co-cultured with *Idh2*-deficient osteoblasts showed reduced TRAP staining compared to WT osteoclast precursors co-cultured with WT osteoblasts, indicating diminished osteoclastogenesis in the absence of *Idh2* (Fig. 4E). A comparable decrease in osteoclastogenesis was observed when osteoclast progenitors were incubated with medium conditioned by mesenchymal stem cells undergoing osteoblast differentiation (Fig. 4D).

3.5. IDH2 regulates RANKL expression in osteoblasts in an ATF4/NFATc1-dependent manner

Next, we examined the effect of IDH2 on mitochondrial functions by analyzing mitochondrial membrane potential (Fig. 5A) and mitochondrial redox status (Fig. 5B) in WT and IDH2-deficient osteoblasts. *Idh2* knockout altered the mitochondrial membrane potential associated with elevated mitochondrial reactive oxygen species (ROS) levels,

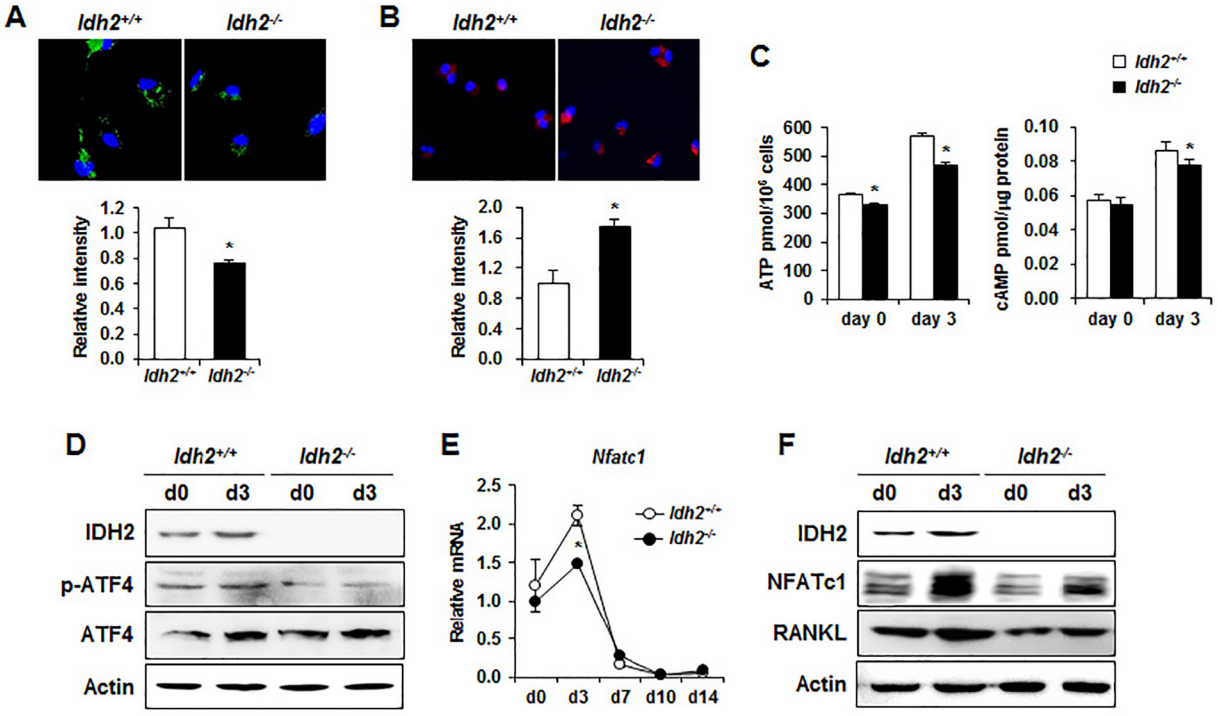

Fig. 5. IDH2 deficiency impairs mitochondrial activity, resulting in reduced RANKL expression via the ATP-ATF4-NFATc1 axis. (A) Mitochondrial membrane potential was measured using rhodamine-123 staining and (B) mitochondrial ROS generation was determined using MitoSox in *Idh2*$^{+/+}$ or *Idh2*$^{-/-}$ osteoblasts cultured in differentiation medium. Each bar graph shows the mean fluorescence intensity relative to that of control. (C) ATP and cAMP levels were measured on days 0 and 3 of osteoblast differentiation. (D) Immunoblot analysis of IDH2, p-ATF4, and ATF4 on days 0 and 3 of osteoblast differentiation. (E) *Nfatc1* mRNA expression level during osteoblast differentiation quantified by qPCR. (F) Immunoblot analysis of IDH2, NFATc1, and RANKL on days 0 and 3 of osteoblast differentiation. Data are represented as the mean ± SD of three independent experiments conducted in triplicate. *$P < 0.05$ versus control.

strongly suggesting that a decrease in the level of ATP and its derivative cAMP content was attributable to alterations in mitochondrial functions seen in IDH2-deficient mice. We measured the levels of ATP and cAMP in osteoblasts cultured under differentiation conditions. As expected, the ATP and cAMP levels in the IDH2-deficient osteoblasts were lower than those in WT osteoblasts, with a prominent difference on day 3 of differentiation (Fig. 5C), correlating with the reduced RANKL expression on day 3 in *Idh2*$^{-/-}$ osteoblasts. Because ATP and cAMP play essential roles in the regulation of transcriptional activity of the cAMP response element-binding protein (CREB), and ATF4, another CREB family member, has been reported to regulate RANKL expression in combination with NFATc1, one of target genes of ATF4 in osteoblasts, we examined changes in phosphorylated (p-) ATF4 and the expression of NFATc1. The level of p-ATF4 on day 3 of osteoblast differentiation was reduced in *Idh2*$^{-/-}$ cells compared to WT cells (Fig. 5D). The level of *Nfatc1* mRNA expression was also reduced in *Idh2*$^{-/-}$ osteoblasts (Fig. 5E), which is similar to the pattern observed with *RANKL* mRNA expression (Fig. 4A). Accordingly, the levels of NFATc1 and RANKL protein in *Idh2*$^{-/-}$ osteoblasts on day 3 of differentiation were lower than those in WT osteoblasts (Fig. 5F). Taken together, these data indicate that the loss of IDH2 results in impaired mitochondrial function with decreased membrane potential and increased mitochondrial ROS levels, leading to decreased ATP production and cAMP-dependent NFATc1/ATF4 signaling in the early stages of osteoblast differentiation, which in turn diminishes RANKL expression, thereby suppressing osteoclastogenesis and resorption activity.

3.6. IDH2 deficiency reduces bone loss in mice with OVX-induced osteoporosis

Next, we determined whether the inhibition of osteoclast differentiation and bone resorption due to IDH2 inactivation protects against bone loss in osteoporosis. A mouse model of OVX-induced osteoporosis was used to determine the importance of IDH2 in postmenopausal osteoporosis. OVX led to a significant decrease in the bone mass of WT mice, as indicated by the 36% decrease in BV/TV measured using μCT analysis, whereas *Idh2*$^{-/-}$ mice were less affected, experiencing only a 21% decrease (Fig. 6A, B). *Idh2*$^{-/-}$ mice were protected from OVX-induced bone loss, indicating that IDH2 deficiency was closely associated with preventing the enhanced osteoclast-mediated bone resorption that occurs following OVX in WT mice. OVX caused a significant increase in osteoclast numbers on the bone surface in WT mice, but this increase was less significant in *Idh2*$^{-/-}$ mice (Fig. 6C). There was no difference in osteoblast numbers on the bone surface between two genotypes (Fig. 6D). BFR was not also altered in either sham or OVX-induced *Idh2*$^{+/+}$ and *Idh2*$^{-/-}$ mice (Supplementary Fig. S4). The prevention of OVX-induced osteoporosis in *Idh2*$^{-/-}$ mice was confirmed by reduced *Tnfsf11* (Fig. 6E) and RANKL (Fig. 6F) expression. Taken together, these data indicate that the loss of IDH2 leads to a decrease in RANKL expression, which in turn reduces osteoclast number and activity, finally resulting in a protective effect against osteoporosis.

4. Discussion

Mitochondrial NADP$^+$-dependent isocitrate dehydrogenase, encoded by *Idh2*, plays a critical role in the regulation of mitochondrial functions, including intermediary metabolism and energy production [26–28]. Although many studies focus on its role in mitochondrial function, the role of IDH2 in bone formation and remodeling has not been studied. To elucidate the function of IDH2 in bone tissue, we analyzed *Idh2*-knockout C57BL/6 mice. We found that IDH2-deficient mice had a high bone mass phenotype associated with decreased numbers of osteoclasts on bone surfaces and decreased osteoclast resorption activity in vivo. However, IDH2 deficiency did not result in any significant changes in osteoclast differentiation and resorption activity in vitro. Therefore, targeting of IDH2-mediated cellular signaling

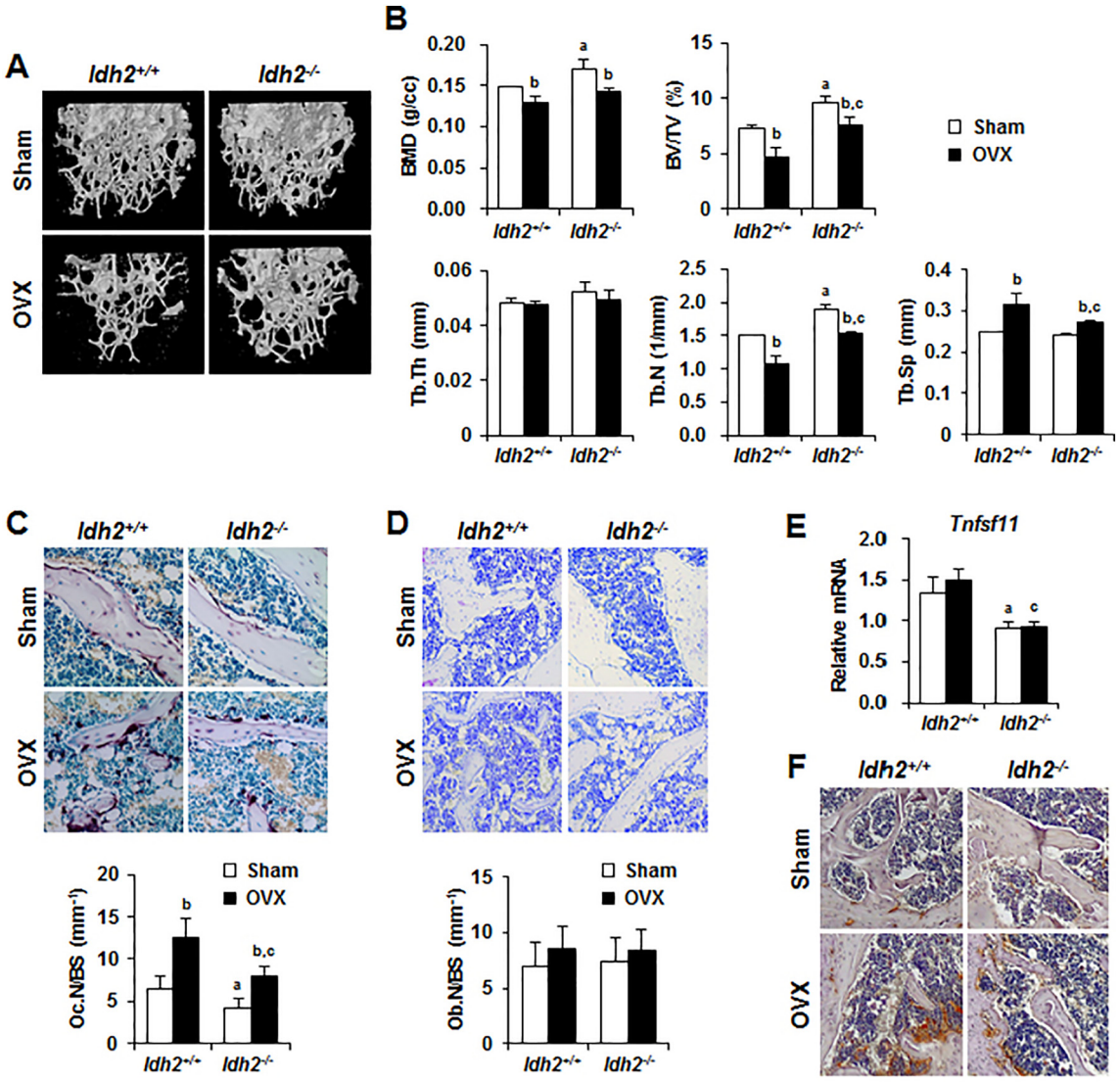

Fig. 6. OVX-induced bone loss is attenuated in *Idh2*$^{-/-}$ mice. (A) μCT reconstructed 3D images of trabecular bone from the distal femur in *Idh2*$^{+/+}$ and *Idh2*$^{-/-}$ mice that were either sham-operated (sham) or ovariectomized (OVX). (B) Structural parameters were assessed using μCT. (C) TRAP-stained femur with quantitative histomorphometry of osteoclast number normalized to the bone surface (Oc.N/BS) and (D) toluidine blue-stained femur with calculated cuboidal osteoblast number per bone surface (Ob.N/BS). (E) *Tnfsf11* (encoding RANKL) expression quantified by qPCR. (F) Immunohistochemistry of RANKL protein expression in femurs from either sham or OVX-induced *Idh2*$^{+/+}$ and *Idh2*$^{-/-}$ mice. Data are represented as the mean ± SD; n = 4 per group. ^{a,b,c} $P < 0.05$. ^{a} *Idh2*$^{-/-}$ Sham versus *Idh2*$^{+/+}$ Sham; ^{b} OVX versus Sham in the same genotype; ^{c} *Idh2*$^{-/-}$ OVX versus *Idh2*$^{+/+}$ OVX. (For interpretation of the references to colour in this figure legend, the reader is referred to the web version of this article.)

needs to be considered in the context of the interaction between bone cells and factors involved in the process of bone remodeling.

Bone remodeling is controlled by multiple local and systemic factors that are responsible for the tightly coupled temporal and spatial interplay between bone-resorbing osteoclasts and bone-forming osteoblasts that maintain bone mass and integrity [1,2,4,5]. RANKL and M-CSF, expressed by the osteoblastic cells, are essential factors for further differentiation, maturation, function, and survival of osteoclasts [14,15]. While M-CSF promotes proliferation and survival of osteoclast precursor cells [42], RANKL directly controls the differentiation and function of osteoclasts by binding to its receptor, RANK, which is expressed in osteoclast lineage cells [43]. Furthermore, osteoblasts and stromal cells synthesize OPG, which is a decoy receptor for RANKL [44]. Thus, the balance between RANKL and OPG expression levels is crucial for regulating osteoclast differentiation and function. We found a marked decrease in levels of RANKL protein in serum and in *Tnfsf11* (RANKL-encoding gene) mRNA expression in bone tissue, while the levels of OPG protein in serum and the levels of *Tnfrsf11b* (OPG-encoding gene) mRNA in bone tissue remained unchanged. These findings indicate that IDH2 deficiency leads to the downregulation of RANKL expression, which explains why both decreased osteoclast number and resorption activity lead to increased bone mass and protection against OVX-induced bone loss.

NFATc1 acts as a master transcriptional regulator in osteoclast differentiation [45]. The binding of RANKL to its receptor RANK on osteoclast precursor cells induces NFATc1 expression and activates osteoclast marker gene transcription. For example, embryonic stem cell lines with an NFATc1 deficiency fail to differentiate into osteoclasts [46,47]. In addition to the effect of NFATc1 in osteoclast lineage cells, several studies report that NFATs play a crucial role in osteoblast-mediated regulation of osteoclast differentiation. Mice that constitutively express nuclear NFATc1 in osteoblasts show elevated osteoclast number and bone resorption activity [48]. NFAT also plays a critical role in isoproterenol-induced RANKL expression in mouse osteoblastic cells [49]. RANKL expression is increased in both a cAMP/PKA- and calcineurin/NFAT-dependent manner, and CREB and NFAT

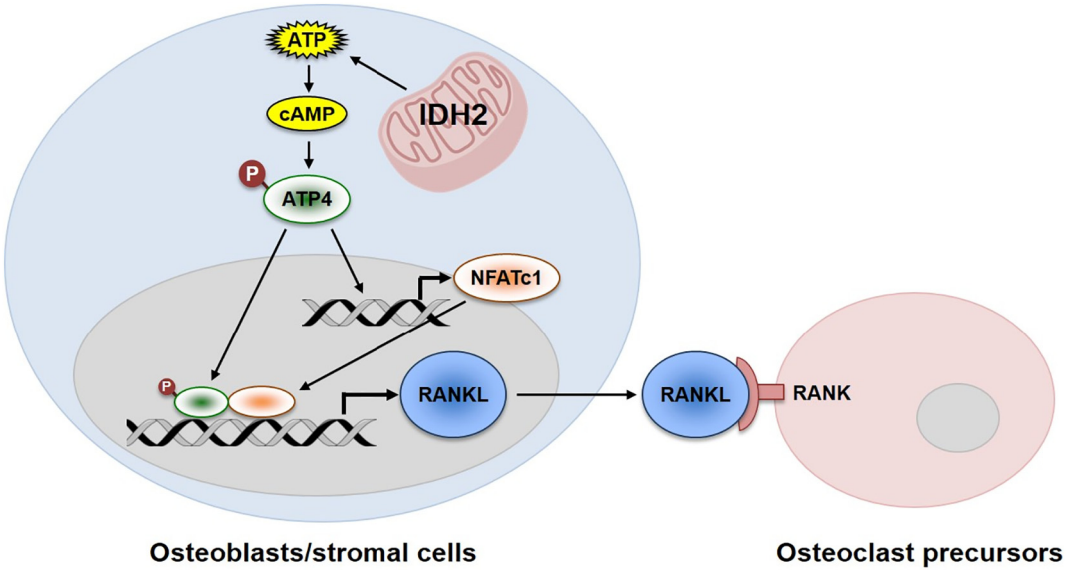

Fig. 7. Proposed model of osteoblast-to-osteoclast crosstalk governed by IDH2. IDH2 regulates the RANKL expression though cAMP-ATF4-NFATc1 signaling pathway in osteoblasts/stromal cells.

cooperate functionally at the RANKL promoter, which is also required for parathyroid hormone related-protein (PTHrP)-induced RANKL expression in osteoblastic cells [50].

Activated CREB mediates parathyroid hormone 1 receptor (PTH1R)-induced RANKL expression by binding to multiple distal enhancers of the *RANKL* gene [51,52]. CREB2, also known as ATF4, is a critical transcription factor in osteoblast differentiation, including the induction of RANKL expression, which is activated in an ATF4-NFATc1 dependent manner [49]. Accordingly, we found that IDH2 regulates RANKL expression through ATF4-NFATc1 signaling in osteoblasts. We measured cellular ATP and cAMP as well as mitochondrial membrane potential to determine the mitochondrial function. The increase in ATP production on day 3 of differentiation in osteoblasts/stromal cells was reduced in IDH2-deficient cells. Consequently, the utilization of ATP and cAMP for the phosphorylation and activation of ATF4 was also decreased, resulting in down-regulated RANKL expression in the early stages of osteoblast differentiation.

Various studies have reported that mitochondrial ROS are key mediators of the communication between mitochondria and the cell in the regulation of homeostasis and maintenance of normal cellular function [53,54]. IDH2 plays an important role in the control of redox balance and oxidative stress levels, which are tightly correlated with intermediary metabolism and energy production. Moreover, there is abundant evidence supporting a general role for IDH2 in the relationship between mitochondrial redox status and the regulation of essential signaling pathways, such as p53, MAP kinase, NF-κB, and AMPK, that control cell growth and differentiation, cell death, and metabolism [41,55,56]. Many recent reports indicate that α-KG, an intermediate metabolite generated by IDH2, is a cofactor for both the Jumonji domain-containing histone demethylases and the TET family of DNA demethylases. Thus, α-KG regulates gene expression through epigenetic controls [57,58]. Therefore, although we provide evidence that ATF4-NFATc1-RANKL signaling in osteoblasts is a primary mediator of the consequences of IDH2 deficiency in controlling bone mass via RANKL-mediated osteoclast differentiation and function, we do not exclude the possibility that other signaling pathways, such as ROS-mediated cellular responses or α-KG-mediated epigenetic control of gene expressions, may also be modulated by IDH2 in osteoblasts. Additional studies are required to elucidate answers to this important question.

Taken together, we have shown that the high bone mass phenotype of IDH2-deficient mice is likely attributable to reduced bone resorption, which is closely associated with the downregulation of RANKL in osteoblasts. As depicted in Fig. 7, our findings suggest that IDH2 is a novel regulator of osteoblast-to-osteoclast communication, at least in part via the ATF4-NFATc1-RANKL signaling axis in osteoblasts. This study demonstrates that IDH2 is a novel regulator of bone mass through osteoblastic modulation on osteoclast activity and provides new perspectives to further investigate the clinical conditions in which small molecule IDH2 inhibitors may protect bone mass, particularly for the treatment of bone loss and osteoporosis.

Declaration of competing interest

All authors state that they have no conflicts of interest.

Acknowledgments

This research was supported by a grant of the Korean Health Technology R&D Project, Ministry of Health and Welfare, Republic of Korea (HI13C1874) and NRF (National Research Foundation of Korea) Grant funded by the Korean Government (NRF-2017-Fostering Core Leaders of the Future Basic Science Program/Global Ph.D. Fellowship Program).

Authors' roles

S.H.L, S.-H.L, J.H.L, J.-W·P, and J.-E.K contributed to the conception and design of the research. S.H.L and S.-H.L performed the experiments, analyzed the data, and interpreted the results of the experiments. S.H.L and J.-E.K prepared the figures, and drafted, edited, and reviewed the manuscript.

Appendix A. Supplementary data

Supplementary data to this article can be found online at https://doi.org/10.1016/j.bone.2019.115056.

References

[1] S. Khosla, J.J. Westendorf, M.J. Oursler, Building bone to reverse osteoporosis and repair fractures, J. Clin. Invest. 118 (2008) 421–428, https://doi.org/10.1172/JCI33612.
[2] X. Feng, J.M. McDonald, Disorders of bone remodeling, Annu. Rev. Pathol. 6 (2011)

121–145, https://doi.org/10.1146/annurev-pathol-011110-130203.
[3] T.J. Martin, E. Seeman, Bone remodelling: its local regulation and the emergence of bone fragility, Best Pract. Res. Clin. Endocrinol. Metab. 22 (2008) 701–722, https://doi.org/10.1016/j.beem.2008.07.006.
[4] L.J. Raggatt, N.C. Partridge, Cellular and molecular mechanisms of bone remodeling, J. Biol. Chem. 285 (2010) 25103–25108, https://doi.org/10.1074/jbc.R109.041087.
[5] M. Zaidi, Skeletal remodeling in health and disease, Nat. Med. 13 (2007) 791–801, https://doi.org/10.1038/nm1593.
[6] D.V. Novack, G. Mbalaviele, Osteoclasts-key players in skeletal health and disease, Microbiol. Spectr. 4 (2016), https://doi.org/10.1128/microbiolspec.MCHD-0011-2015.
[7] V. Everts, T.J. de Vries, M.H. Helfrich, Osteoclast heterogeneity: lessons from osteopetrosis and inflammatory conditions, Biochim. Biophys. Acta 1792 (2009) 757–765, https://doi.org/10.1016/j.bbadis.2009.05.004.
[8] C. Sobacchi, A. Schulz, F.P. Coxon, A. Villa, M.H. Helfrich, Osteopetrosis: genetics, treatment and new insights into osteoclast function, Nat. Rev. Endocrinol. 9 (2013) 522–536, https://doi.org/10.1038/nrendo.2013.137.
[9] C.S. Thudium, I. Moscatelli, C. Flores, J.S. Thomsen, A. Brüel, N.S. Gudmann, E.-M. Hauge, M.A. Karsdal, J. Richter, K. Henriksen, A comparison of osteoclast-rich and osteoclast-poor osteopetrosis in adult mice sheds light on the role of the osteoclast in coupling bone resorption and bone formation, Calcif. Tissue Int. 95 (2014) 83–93, https://doi.org/10.1007/s00223-014-9865-4.
[10] K. Henriksen, J. Bollerslev, V. Everts, M.A. Karsdal, Osteoclast activity and subtypes as a function of physiology and pathology–implications for future treatments of osteoporosis, Endocr. Rev. 32 (2011) 31–63, https://doi.org/10.1210/er.2010-0006.
[11] E. Seeman, P.D. Delmas, Bone quality — the material and structural basis of bone strength and fragility, N. Engl. J. Med. 354 (2006) 2250–2261, https://doi.org/10.1056/NEJMra053077.
[12] X. Chen, Z. Wang, N. Duan, G. Zhu, E.M. Schwarz, C. Xie, Osteoblast-osteoclast interactions, Connect. Tissue Res. 59 (2018) 99–107, https://doi.org/10.1080/03008207.2017.1290085.
[13] H. Enomoto, S. Shiojiri, K. Hoshi, T. Furuichi, R. Fukuyama, C.A. Yoshida, N. Kanatani, R. Nakamura, A. Mizuno, A. Zanma, K. Yano, H. Yasuda, K. Higashio, K. Takada, T. Komori, Induction of osteoclast differentiation by Runx2 through receptor activator of nuclear factor-κB ligand (RANKL) and osteoprotegerin regulation and partial rescue of osteoclastogenesis in Runx2−/− mice by RANKL transgene, J. Biol. Chem. 278 (2003) 23971–23977, https://doi.org/10.1074/jbc.M302457200.
[14] M. Karst, G. Gorny, R.J.S. Galvin, M.J. Oursler, Roles of stromal cell RANKL, OPG, and M-CSF expression in biphasic TGF-beta regulation of osteoclast differentiation, J. Cell. Physiol. 200 (2004) 99–106, https://doi.org/10.1002/jcp.20036.
[15] B.F. Boyce, L. Xing, Functions of RANKL/RANK/OPG in bone modeling and remodeling, Arch. Biochem. Biophys. 473 (2008) 139–146, https://doi.org/10.1016/j.abb.2008.03.018.
[16] W.-C. Lee, A.R. Guntur, F. Long, C.J. Rosen, Energy metabolism of the osteoblast: implications for osteoporosis, Endocr. Rev. 38 (2017) 255–266, https://doi.org/10.1210/er.2017-00064.
[17] Q. Li, Z. Gao, Y. Chen, M.-X. Guan, The role of mitochondria in osteogenic, adipogenic and chondrogenic differentiation of mesenchymal stem cells, Protein Cell 8 (2017) 439–445, https://doi.org/10.1007/s13238-017-0385-7.
[18] L.C. Shum, N.S. White, B.N. Mills, K.L. de Mesy Bentley, R.A. Eliseev, Energy metabolism in mesenchymal stem cells during osteogenic differentiation, Stem Cells Dev. 25 (2016) 114–122, https://doi.org/10.1089/scd.2015.0193.
[19] J.H. An, J.-Y. Yang, B.Y. Ahn, S.W. Cho, J.Y. Jung, H.Y. Cho, Y.M. Cho, S.W. Kim, K.S. Park, S.Y. Kim, H.K. Lee, C.S. Shin, Enhanced mitochondrial biogenesis contributes to Wnt induced osteoblastic differentiation of C3H10T1/2 cells, Bone 47 (2010) 140–150, https://doi.org/10.1016/j.bone.2010.04.593.
[20] S.V. Komarova, F.I. Ataullakhanov, R.K. Globus, Bioenergetics and mitochondrial transmembrane potential during differentiation of cultured osteoblasts, Am. J. Physiol. Cell Physiol. 279 (2000) C1220–C1229, https://doi.org/10.1152/ajpcell.2000.279.4.C1220.
[21] K. Ikeda, S. Takeshita, The role of osteoclast differentiation and function in skeletal homeostasis, J. Biochem. 159 (2016) 1–8, https://doi.org/10.1093/jb/mvv112.
[22] S. Lemma, M. Sboarina, P.E. Porporato, N. Zini, P. Sonveaux, G. Di Pompo, N. Baldini, S. Avnet, Energy metabolism in osteoclast formation and activity, Int. J. Biochem. Cell Biol. 79 (2016) 168–180, https://doi.org/10.1016/j.biocel.2016.08.034.
[23] S.S. Gandhi, C. Muraresku, E.M. McCormick, M.J. Falk, S.E. McCormack, Risk factors for poor bone health in primary mitochondrial disease, J. Inherit. Metab. Dis. 40 (2017) 673–683, https://doi.org/10.1007/s10545-017-0046-2.
[24] H. Kato, X. Han, H. Yamaza, K. Masuda, Y. Hirofuji, H. Sato, T.T.M. Pham, T. Taguchi, K. Nonaka, Direct effects of mitochondrial dysfunction on poor bone health in Leigh syndrome, Biochem. Biophys. Res. Commun. 493 (2017) 207–212, https://doi.org/10.1016/j.bbrc.2017.09.045.
[25] S.S. Papiha, H. Rathod, I. Briceno, J. Pooley, H.K. Datta, Age related somatic mitochondrial DNA deletions in bone, J. Clin. Pathol. 51 (1998) 117–120, https://doi.org/10.1136/jcp.51.2.117.
[26] R.J. Haselbeck, L. McAlister-Henn, Function and expression of yeast mitochondrial NAD- and NADP-specific isocitrate dehydrogenases, J. Biol. Chem. 268 (1993) 12116–12122.
[27] L.A. Sazanov, J.B. Jackson, Proton-translocating transhydrogenase and NAD- and NADP-linked isocitrate dehydrogenases operate in a substrate cycle which contributes to fine regulation of the tricarboxylic acid cycle activity in mitochondria, FEBS Lett. 344 (1994) 109–116, https://doi.org/10.1016/0014-5793(94)00370-X.
[28] M.J. MacDonald, L.J. Brown, M.J. Longacre, S.W. Stoker, M.A. Kendrick, N.M. Hasan, Knockdown of both mitochondrial isocitrate dehydrogenase enzymes in pancreatic beta cells inhibits insulin secretion, Biochim. Biophys. Acta 1830 (2013) 5104–5111, https://doi.org/10.1016/j.bbagen.2013.07.013.
[29] S.-H. Jo, M.-K. Son, H.-J. Koh, S.-M. Lee, I.-H. Song, Y.-O. Kim, Y.-S. Lee, K.-S. Jeong, W.B. Kim, J.-W. Park, B.J. Song, T.-L. Huh, Control of mitochondrial redox balance and cellular defense against oxidative damage by mitochondrial NADP+-dependent isocitrate dehydrogenase, J. Biol. Chem. 276 (2001) 16168–16176, https://doi.org/10.1074/jbc.M010120200.
[30] H.J. Ku, Y. Ahn, J.H. Lee, K.M. Park, J.-W. Park, IDH2 deficiency promotes mitochondrial dysfunction and cardiac hypertrophy in mice, Free Radic. Biol. Med. 80 (2015) 84–92, https://doi.org/10.1016/j.freeradbiomed.2014.12.018.
[31] S.J. Lee, H. Cha, S. Lee, H. Kim, H.J. Ku, S.H. Kim, J.H. Park, J.H. Lee, K.M. Park, J.-W. Park, Idh2 deficiency accelerates renal dysfunction in aged mice, Biochem. Biophys. Res. Commun. 493 (2017) 34–39, https://doi.org/10.1016/j.bbrc.2017.09.082.
[32] H. Kim, S.H. Kim, H. Cha, S.R. Kim, J.H. Lee, J.-W. Park, IDH2 deficiency promotes mitochondrial dysfunction and dopaminergic neurotoxicity: implications for Parkinson's disease, Free Radic. Res. 50 (2016) 853–860, https://doi.org/10.1080/10715762.2016.1185519.
[33] I.R. Orriss, G. Burnstock, T.R. Arnett, Purinergic signalling and bone remodelling, Curr. Opin. Pharmacol. 10 (2010) 322–330, https://doi.org/10.1016/j.coph.2010.01.003.
[34] A. Cutarelli, M. Marini, V. Tancredi, G. D'Arcangelo, M. Murdocca, C. Frank, U. Tarantino, Adenosine triphosphate stimulates differentiation and mineralization in human osteoblast-like Saos-2 cells, Develop. Growth Differ. 58 (2016) 400–408, https://doi.org/10.1111/dgd.12288.
[35] S. Katz, R. Boland, G. Santillán, Modulation of ERK 1/2 and p38 MAPK signaling pathways by ATP in osteoblasts: involvement of mechanical stress-activated calcium influx, PKC and Src activation, Int. J. Biochem. Cell Biol. 38 (2006) 2082–2091, https://doi.org/10.1016/j.biocel.2006.05.018.
[36] N.K. Lee, Y.G. Choi, J.Y. Baik, S.Y. Han, D.W. Jeong, Y.S. Bae, N. Kim, S.Y. Lee, A crucial role for reactive oxygen species in RANKL-induced osteoclast differentiation, Blood 106 (2005) 852–859, https://doi.org/10.1182/blood-2004-09-3662.
[37] H.-J. Moon, S.E. Kim, Y.P. Yun, Y.-S. Hwang, J.B. Bang, J.-H. Park, I.K. Kwon, Simvastatin inhibits osteoclast differentiation by scavenging reactive oxygen species, Exp. Mol. Med. 43 (2011) 605–612, https://doi.org/10.3858/emm.2011.43.11.067.
[38] B. Zhang, Q.Y. Xie, Y. Quan, X.M. Pan, D.F. Liao, Reactive oxygen species induce cell death via Akt signaling in rat osteoblast-like cell line ROS 17/2.8, Toxicol. Ind. Health 31 (2015) 1236–1242, https://doi.org/10.1177/0748233713491801.
[39] J.-R. Chen, O.P. Lazarenko, M.L. Blackburn, K.E. Mercer, T.M. Badger, M.J.J. Ronis, p47^{phox}-Nox2-dependent ROS signaling inhibits early bone development in mice but protects against skeletal aging, J. Biol. Chem. 290 (2015) 14692–14704, https://doi.org/10.1074/jbc.M114.633461.
[40] N. Arakaki, A. Yamashita, S. Niimi, T. Yamazaki, Involvement of reactive oxygen species in osteoblastic differentiation of MC3T3-E1 cells accompanied by mitochondrial morphological dynamics, Biomed. Res. 34 (2013) 161–166.
[41] S.J. Lee, S.H. Kim, K.M. Park, J.H. Lee, J.-W. Park, Increased obesity resistance and insulin sensitivity in mice lacking the isocitrate dehydrogenase 2 gene, Free Radic. Biol. Med. 99 (2016) 179–188, https://doi.org/10.1016/j.freeradbiomed.2016.08.011.
[42] H. Kitaura, P. Zhou, H.J. Kim, D.V. Novack, F.P. Ross, S.L. Teitelbaum, M-CSF mediates TNF-induced inflammatory osteolysis, J. Clin. Invest. 115 (2005) 3418–3427, https://doi.org/10.1172/JCI26132.
[43] N. Udagawa, N. Takahashi, E. Jimi, K. Matsuzaki, T. Tsurukai, K. Itoh, N. Nakagawa, H. Yasuda, M. Goto, E. Tsuda, K. Higashio, M.T. Gillespie, T.J. Martin, T. Suda, Osteoblasts/stromal cells stimulate osteoclast activation through expression of osteoclast differentiation factor/RANKL but not macrophage colony-stimulating factor: receptor activator of NF-kappa B ligand, Bone 25 (1999) 517–523, https://doi.org/10.1016/S8756-3282(99)00210-0.
[44] N. Udagawa, N. Takahashi, H. Yasuda, A. Mizuno, K. Itoh, Y. Ueno, T. Shinki, M.T. Gillespie, T.J. Martin, K. Higashio, T. Suda, Osteoprotegerin produced by osteoblasts is an important regulator in osteoclast development and function, Endocrinology 141 (2000) 3478–3484, https://doi.org/10.1210/endo.141.9.7634.
[45] D. Sitara, A.O. Aliprantis, Transcriptional regulation of bone and joint remodeling by NFAT, Immunol. Rev. 233 (2010) 286–300, https://doi.org/10.1111/j.0105-2896.2009.00849.x.
[46] H. Takayanagi, S. Kim, T. Koga, H. Nishina, M. Isshiki, H. Yoshida, A. Saiura, M. Isobe, T. Yokochi, J. Inoue, E.F. Wagner, T.W. Mak, T. Kodama, T. Taniguchi, Induction and activation of the transcription factor NFATc1 (NFAT2) integrate RANKL signaling in terminal differentiation of osteoclasts, Dev. Cell 3 (2002) 889–901, https://doi.org/10.1016/S1534-5807(02)00369-6.
[47] H. Hirotani, N.A. Tuohy, J.-T. Woo, P.H. Stern, N.A. Clipstone, The Calcineurin/nuclear factor of activated T cells signaling pathway regulates Osteoclastogenesis in RAW264.7 cells, J. Biol. Chem. 279 (2004) 13984–13992, https://doi.org/10.1074/jbc.M213067200.
[48] M.M. Winslow, M. Pan, M. Starbuck, E.M. Gallo, L. Deng, G. Karsenty, G.R. Crabtree, Calcineurin/NFAT signaling in osteoblasts regulates bone mass, Dev. Cell 10 (2006) 771–782, https://doi.org/10.1016/j.devcel.2006.04.006.
[49] K. Baek, H.-J. Park, J.-H. Baek, H.-R. Kim, Isoproterenol increases RANKL expression in a ATF4/NFATc1-dependent manner in mouse osteoblastic cells, Int. J. Mol. Sci. 18 (2017) 2204, https://doi.org/10.3390/ijms18102204.
[50] H.-J. Park, K. Baek, J.-H. Baek, H.-R. Kim, The cooperation of CREB and NFAT is required for PTHrP-induced RANKL expression in mouse osteoblastic cells, J. Cell. Physiol. 230 (2015) 667–679, https://doi.org/10.1002/jcp.24790.

[51] Q. Fu, S.C. Manolagas, C.A. O'Brien, Parathyroid hormone controls receptor activator of NF-kappaB ligand gene expression via a distant transcriptional enhancer, Mol. Cell. Biol. 26 (2006) 6453–6468, https://doi.org/10.1128/MCB.00356-06.
[52] S. Kim, M. Yamazaki, N.K. Shevde, J.W. Pike, Transcriptional control of receptor activator of nuclear factor-kappaB ligand by the protein kinase a activator forskolin and the transmembrane glycoprotein 130-activating cytokine, oncostatin M, is exerted through multiple distal enhancers, Mol. Endocrinol. 21 (2007) 197–214, https://doi.org/10.1210/me.2006-0315.
[53] R.B. Hamanaka, N.S. Chandel, Mitochondrial reactive oxygen species regulate cellular signaling and dictate biological outcomes, Trends Biochem. Sci. 35 (2010) 505–513, https://doi.org/10.1016/j.tibs.2010.04.002.
[54] G.S. Shadel, T.L. Horvath, Mitochondrial ROS signaling in organismal homeostasis, Cell 163 (2015) 560–569, https://doi.org/10.1016/j.cell.2015.10.001.
[55] H.J. Ku, J.-W. Park, Downregulation of IDH2 exacerbates H_2O_2 -mediated cell death and hypertrophy, Redox Rep. 22 (2017) 35–41, https://doi.org/10.1080/13510002.2015.1135581.
[56] J.H. Park, H.J. Ku, J.H. Lee, J.-W. Park, IDH2 deficiency accelerates skin pigmentation in mice via enhancing melanogenesis, Redox Biol. 17 (2018) 16–24, https://doi.org/10.1016/j.redox.2018.04.008.
[57] J.-P. Etchegaray, R. Mostoslavsky, Interplay between metabolism and epigenetics: a nuclear adaptation to environmental changes, Mol. Cell 62 (2016) 695–711, https://doi.org/10.1016/j.molcel.2016.05.029.
[58] W.G. Kaelin Jr., S.L. McKnight, Influence of metabolism on epigenetics and disease, Cell 153 (2013) 56–69, https://doi.org/10.1016/j.cell.2013.03.004.